Physicochemical hazard assessment of ash and dome rock from the 2021 eruption of La Soufrière, St Vincent, for the assessment of respiratory health impacts and water contamination

C. J. Horwell[1]*, D. E. Damby[2], C. Stewart[3], E. P. Joseph[4], J. Barclay[5], B. V. Davies[5], M. F. Mangler[6], L. G. Marvin[7], J. Najorka[8], S. Peek[2] and N. Tunstall[9]

[1]Institute of Hazard, Risk & Resilience, Department of Earth Sciences, Durham University, UK

[2]US Geological Survey, Volcano Science Center, USA

[3]College of Health, Massey University, NZ

[4]University of the West Indies Seismic Research Centre, Trinidad and Tobago

[5]School of Environmental Sciences, University of East Anglia, UK

[6]Department of Earth Sciences, Durham University, UK

[7]School of Geography, Geology and the Environment, University of Leicester, UK

[8]Natural History Museum, UK

[9]Department of Geography, Durham University, UK

CJH, 0000-0002-0148-6933

*Correspondence: claire.horwell@durham.ac.uk

Abstract: La Soufrière, St Vincent, began an extrusive eruption on 27 December 2020. The lava dome was destroyed, along with much of the pre-existing 1979 dome, in explosive eruptions from 9 to 22 April 2021. Lava domes generate crystalline silica – inhalation of which can cause silicosis in occupational settings – which can become hazardous when dome material is incorporated into volcanic ash.

La Soufrière ash (17 samples) was analysed, according to IVHHN protocols, to rapidly quantify crystalline silica and test for other health-relevant properties. The basaltic andesitic ash contained <5 wt% crystalline silica, which agrees with previous analyses of ash of similar compositions and mirrors the low quantities measured in dome samples (2 area %). It contained substantial inhalable material (7–21 vol% <10 μm). Few fibre-like particles were observed, reducing concern about particle shape. Leaching assays found low concentrations of potentially toxic elements, which indicates low potential to impact health, contaminate drinking-water sources or harm grazing animals through ingestion. Collectively, these data indicate that the primary health concern from this eruption was the potential for fine-grained ash to increase ambient particulate matter, an environmental risk factor for respiratory and cardiovascular morbidity and mortality. Precautionary measures were advised to minimize exposure.

Supplementary material: Further methods and leachate analysis information (S1) and particle size (S2) and XRD (S3) data are available at https://doi.org/10.6084/m9.figshare.c.6745583

La Soufrière, St Vincent, began an effusive eruption on 27 December 2020. A lava dome or coulée grew from then until 9 April 2021, when it was destroyed in a series of explosive eruptions, along with around 60% of the pre-existing 1979 dome (Camejo-Harry *et al.* 2023; Cole *et al.* 2023; Morrison-Evans *et al.* 2023). The explosions generated tephra which was dispersed across St Vincent and the surrounding islands. The tephra caused considerable damage to buildings, infrastructure and agriculture, with an accompanying economic impact associated with clean-up, repairs, rebuilding and crop loss, and displacement of the affected communities (Miller *et al.* 2022). Due to the population displacement, health surveillance efforts focused on the spread of communicable diseases in evacuation shelters (the eruption happened in the midst of the Covid-19 pandemic).

Historically, La Soufrière volcano has had both effusive (lava dome building) and explosive basaltic

From: Robertson, R. E. A., Joseph, E. P., Barclay, J. and Sparks, R. S. J. (eds) 2024. *The 2020–21 Eruption of La Soufrière Volcano, St Vincent*. Geological Society, London, Special Publications, **539**, 311–329.
First published online August 23, 2023, https://doi.org/10.1144/SP539-2023-46

andesite eruptions, sometimes switching between these phases during individual eruptive episodes, as happened in 2021 (Joseph *et al.* 2022). Given that both lava domes and explosions can generate hazards that may impact human health, a rapid assessment of the respiratory health hazards of the eruptive products from the 2021 eruption was warranted. This could be achieved through a suite of physicochemical analyses of hazardous ash characteristics, through a protocol developed by the International Volcanic Health Hazard Network (IVHHN 2023).

The *potential* health impacts from exposure to volcanic emissions can be categorized into (1) acute (short-term) impacts – primarily temporary symptoms – caused by acute exposures to ash and gas and (2) chronic impacts – usually meaning serious, sometimes fatal respiratory diseases – caused by longer exposures, either continuous or intermittent, over a period of months to years. Such diseases could develop decades after exposure ends, as with cigarette smoking-related lung cancer and mesothelioma from asbestos exposures (e.g. Leung *et al.* 2012; Frost 2013; Lipfert and Wyzga 2019).

Acute exposures to volcanic ash, gas and aerosol may cause throat/lung irritation, cough and bronchitic symptoms in healthy people whereas individuals with respiratory diseases (e.g. asthma, bronchitis and chronic obstructive pulmonary disease (COPD)) may experience exacerbation of pre-existing symptoms (Horwell and Baxter 2006; Stewart *et al.* 2022). A study of communities exposed to the ash generated in the 1979 eruption of La Soufrière was the first (globally) to identify that inhalation of volcanic ash triggered acute asthmatic bronchitis, especially in children under two years old (Leus *et al.* 1981).

The primary risk of chronic disease from inhalation of volcanic ash is through exposure to respirable crystalline silica. In occupational settings, crystalline silica inhalation can cause the fibrotic lung disease silicosis, and lung cancer, in workers exposed to such mineral dusts (International Agency for Research on Cancer 1997). Research has shown that it is common (if not ubiquitous) for lava domes to generate a form of crystalline silica, cristobalite, which crystallizes from vapours in cracks and vesicles (known as vapour-phase crystallization) and by devitrification (the process of crystallization of groundmass glass) (Dollberg *et al.* 1986; Baxter *et al.* 1999; Damby 2012; Horwell *et al.* 2013*a*). Quartz, another form of crystalline silica, is also found in volcanic rocks but is not common in magmas of basaltic andesite composition due to their relatively low bulk SiO_2 content. Therefore, at St Vincent, lava domes are presumed to be the primary source of crystalline silica. To date, however, no causal association between volcanic ash exposure and silicosis (or any other chronic lung disease) has been proven, and there is good evidence that impurities in and on the surface of volcanic crystalline silica particles may inhibit their toxicity (Horwell *et al.* 2012; Nattrass *et al.* 2017). Particle toxicology assays with crystalline-silica-rich ash have also shown limited cytotoxicity (cell injury or death), although there is evidence of an inflammatory response in both *in vitro* and *in vivo* studies (Lee and Richards 2004; Damby *et al.* 2016, 2018). Nevertheless, until definitive clinical evidence becomes available, crystalline silica in volcanic ash is still regarded as a serious risk to communities and, if substantial concentrations are confirmed, precautionary measures may be recommended to minimize inhalational exposure, and medical surveillance initiated.

With a new lava dome growing in early 2021, and an existing lava dome (from 1979) also present in the crater, there was a significant chance that explosive activity might commence which would at least disrupt, and possibly destroy, both domes. So, it was prudent to ascertain how much crystalline silica was in the dome material, prior to the onset of explosive activity, to give an indication of likely crystalline silica content of the ash if an explosive phase ensued. In March and early April 2021, we petrographically analysed lava dome rock samples from both archived 1979 dome material and the new 2020–21 La Soufrière dome, collected in January 2021. Once explosive ash generation started, in April 2021, crystalline silica content was quantified in the ash samples.

Ash can have other potentially harmful physicochemical characteristics, in addition to the presence and quantity of crystalline silica. Firstly, fine particles in themselves – particularly <2.5 μm diameter but also <10 μm diameter – are classed as carcinogenic and capable of contributing to a range of morbidities and early mortality (Loomis *et al.* 2013; World Health Organization 2013). The World Health Organization's review of evidence on health aspects of air pollution (REVIHAAP) concluded that crustal particles posed the same risks as anthropogenic particulate, while acknowledging that there was insufficient evidence to classify them separately (World Health Organization 2013). Therefore, it is important to characterize the size of ash in terms of the percentage fraction of particles that are able to enter the respiratory system (the 'inhalable' fraction; <100 μm diameter), penetrate beyond the larynx (the 'thoracic' fraction; <10 μm diameter), penetrate beyond the ciliated airways into the alveoli (the 'respirable' fraction; <4 μm diameter), and the <2.5 and <1 μm fractions (which are considered the most pathogenic (e.g. MacNee and Donaldson 2003) and, also, could translocate around the body and settle in other organs). Ideally, the

concentrations of these fractions would be measured when they are airborne, but ambient or personal (occupational) particulate monitoring is rarely in place in areas affected by airborne volcanic hazards. There was no air quality monitoring on St Vincent at the time of the 2021 explosive eruptions. Therefore, as is common in volcanic crises, settled deposits of ash were used for the analyses for this study, with particle size distributions measured using laser diffraction. Using such 'bulk' ash also has the advantage that there is usually sufficient sample not only for particle size analysis but also for a suite of other physicochemical analyses, which is not possible when particles are collected through airborne sampling (if particulate is even collected which, for most air quality monitoring techniques, it is not).

In addition to particle size, there is often concern about the shape of volcanic ash particles. Fibrous particles (considered to have a long axis >5 µm and an aspect ratio $>3{:}1$ (World Health Organization 1997)) have an elongate shape, which affects both deposition and retention in the lungs. Such fibres can cause 'frustrated phagocytosis' in the macrophages tasked with removing particles from the lungs (Schinwald *et al.* 2012; Ishida *et al.* 2019). This failed clearance of reactive particles can lead to diseases, such as mesothelioma for asbestos (Schinwald *et al.* 2012). While most volcanic ash particles are not elongate, fibre-like cristobalite has been documented (Reich *et al.* 2009) and some volcanic explosions can mobilize (from hydrothermal systems) or generate fibre-like particles, such as anhydrite/gypsum (e.g. Delmelle *et al.* 2007; Horwell *et al.* 2008, 2013*b*; Le Blond *et al.* 2010; Ayris *et al.* 2013). Sparse silicate/glass fibre-like particles have also been observed in ash (Le Blond *et al.* 2010; Horwell *et al.* 2010*a*, 2013*a*), although, to date, concerning quantities of such particles have not been documented in ash from large explosive eruptions, so they are unlikely to cause a specific impact (Horwell *et al.* 2013*b*). No asbestos-related particles have been observed in fresh volcanic ash (e.g. Le Blond *et al.* 2010; Horwell *et al.* 2010*b*, 2013*a*; Damby *et al.* 2013). Given that La Soufrière's explosive eruptions disrupted the 1979 lava dome and edifice, which may have undergone hydrothermal alteration (Cole *et al.* 2023), particle shape was also checked in this study.

Elements that may readily leach from ash surfaces may be tested for several reasons. Of importance to respiratory assessment is that potentially toxic elements (PTEs) may leach into lung fluids (Tomašek *et al.* 2021). However, a greater hazard is the potential for elements to leach from ash into drinking water, making it either unpalatable or, more unusually, raising concentrations of elements such as F (as fluoride) above health-based drinking-water standards. Additionally, protecting animal health is of great importance and grazing animals may ingest substantial quantities of ash following an eruption, from which PTEs may leach in gastrointestinal fluids. Analyses were conducted for all three purposes using a leachate protocol specifically developed for volcanic ash by IVHHN (Stewart *et al.* 2020).

As mentioned, the above analyses/protocols are part of a broader protocol for rapid characterization of ash for assessment of respiratory hazard (Fig. 1), developed by IVHHN. A number of previous studies have utilized these protocols, allowing comparison among the St Vincent samples and eruptions elsewhere (Le Blond *et al.* 2010; Horwell *et al.* 2010*a*, 2013*b*; Hillman *et al.* 2012; Damby *et al.* 2013, 2017). The rapid assessment protocol contains some methods that were not utilized during the St Vincent eruption (Fig. 1). During an eruption crisis, it is essential to conduct analyses as rapidly as possible so that urgent public health decisions may be made, and interventions implemented, on community protection and exposure reduction. In this case, bulk composition analyses of the ash were not conducted during the eruption crisis as it was already known from analysis of the lava dome that the initial magma was basaltic andesite in composition – as expected for this volcano (Huppert *et al.* 1982; Robertson 2005; Cole *et al.* 2019; Joseph *et al.* 2022; Morrison-Evans *et al.* 2023; Weber *et al.* 2023). However, bulk compositional analyses were conducted on the ash samples after the crisis so that the samples could be set in the context of IVHHN ash analyses of other eruptions. Based on the results of the crystalline silica quantification (see Results section), a decision was made not to conduct any toxicological analyses and particle size findings were used as a proxy for specific surface area, which is sometimes measured (see Fig. 1), as surface area may correlate with toxicity of particles (e.g. Schmid and Stoeger 2016).

Methods

Sample collection and preparation

Eight samples of dome rock were collected from a single lobe at the margin of the growing 2020–21 lava dome on 16 January 2021 by the University of the West Indies Seismic Research Centre (UWI SRC). The dome samples used for this study, from sub-sample SVG-2021/16, were thin sectioned and carbon coated at the University of Granada and Durham University (DU).

A single thin section of 1979 dome lava was supplied by the University of Oxford (section #7060). The lava was collected on 20 May 1979, shortly after extrusion, by John Tomblin and was sourced from the University of Oxford's archives.

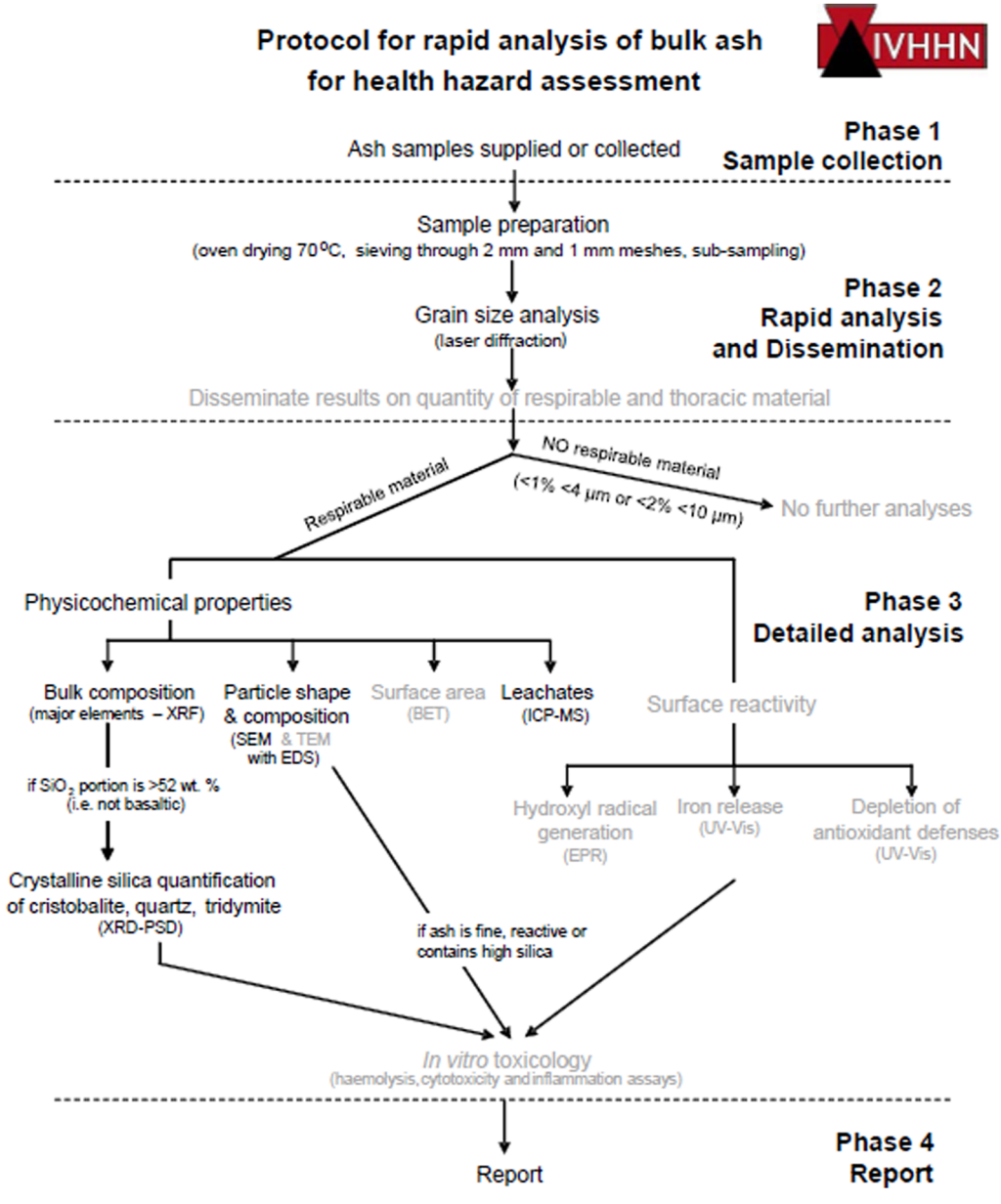

Fig. 1. IVHHN protocol for rapid ash analysis for health hazard assessment. Black text indicates analyses conducted for this study. Grey text indicates analyses not conducted. Bulk composition by XRF was conducted after the eruption response.

Seventeen samples of volcanic ash were collected on St Vincent and Barbados (Table 1; Fig. 2). Samples SV_01–SV_15 were collected on St Vincent; samples BB_01 and BB_02 were collected on Barbados. Samples SV_01, 02, 04, 06–15 and BB_01 were collected from ash that fell from the initial explosions (9–11 April), when the domes were destroyed (9–10 April). Sample BB_02 was collected from ash that fell on 12 April. Samples SV_03 and SV_05 are thought to have fallen on or after 11 April. The explosions after 11 April are presumed to have occurred after most of the domes were destroyed. Samples SV_06–SV_12 were collected from a stratigraphic sequence from a deposit at

Table 1. *Ash sample information*

Ash sample #	Island of deposit	Collected by (organization)	Location of collection	Latitude/Longitude	Date of collection	Source eruption	Further information	Original sample #
SV_01	St Vincent	UWI SRC*	Field on the side of road, Rabacca (river mouth)	13.3001750,−61.1169028	10 April 2021	9–10 April 2021	Dry sample; whole deposit sampled from grassy soil	Sample 1
SV_02	St Vincent	UEA[†]/ Plymouth[‡]	Barrouallie	13.2490926,−61.2636521	1 May 2021	*c.* 9–11 April 2021	Lower few mm of 1 cm deposit. Wall top	LS21-CH1 (LSL20)
SV_03	St Vincent	UEA/Plymouth	Barrouallie	13.2490926,−61.2636521	1 May 2021	*c.* 11–22 April 2021	Upper few mm of 1 cm deposit. Wall top	LS21-CH2 (LSL20)
SV_04	St Vincent	UEA/Plymouth	Troumaca	13.2785802,−61.2563822	3 May 2021	*c.* 9–11 April 2021	Lower 3.5 cm of deposit. Wall top	LS21-CH3/46
SV_05	St Vincent	UEA/Plymouth	Troumaca	13.2785802,−61.2563822	3 May 2021	*c.* 11–22 April 2021	Upper cm of 3.5 cm deposit. Wall top	LS21-CH4/48
SV_06	St Vincent	UEA	Richmond Vale Academy	13.3113962,−61.2296795	26 April 2021	10–11 April 2021	U6; U6 total = 20 mm. AC. Table top	LS21–1
SV_07	St Vincent	UEA	Richmond Vale Academy	13.3113962,−61.2296795	26 April 2021	10–11 April 2021	U5 coarse; U5 total = 20 mm. AC. Table top	LS21-2
SV_08	St Vincent	UEA	Richmond Vale Academy	13.3113962,−61.2296795	26 April 2021	10–11 April 2021	U3 fine ash; U3 total = 20 mm. AC. Table top	LS21-3
SV_09	St Vincent	UEA	Richmond Vale Academy	13.3113962,−61.2296795	26 April 2021	10–11 April 2021	U3 double lapilli layer couplet; U3 total = 20 mm. Table top	LS21-4
SV_10	St Vincent	UEA	Richmond Vale Academy	13.3113962,−61.2296795	26 April 2021	10 April 2021	U2 grey layer; U2 total = 40 mm. Table top	LS21-5
SV_11	St Vincent	UEA	Richmond Vale Academy	13.3113962,−61.2296795	26 April 2021	10 April 2021	U2 buff layer; U2 total = 40 mm. Table top	LS21-6
SV_12	St Vincent	UEA	Richmond Vale Academy	13.3113962,−61.2296795	26 April 2021	9–10 April 2021	U1: lapilli deposit – 5 mm. Table top	LS21-7
SV_13	St Vincent	JT[§]	Jenny's Place, Ratho Mill	13.1283672,−61.1919708	10 April 2021	10 April 2021	Dry sample of initial fallout up to 05:40 ECT	LS21-63
SV_14	St Vincent	JT	Jenny's Place, Ratho Mill	13.1283672,−61.1919708	10 April 2021	10 April 2021	Dry sample of fallout between 05:40 and 12:00 ECT	LS21-64
SV_15	St Vincent	JT	Jenny's Place, Ratho Mill	13.1283672,−61.1919708	10 April 2021	10 April 2021	Dry sample of fallout between 12:00–14:00 ECT	LS21-65
BB_01	Barbados	UK FCDO[¶]	House to north of island	13.3272547,−59.6151712	10 April 2021	9–10 April 2021	Dry sample; Ash collected from 25 × 25 cm tiled table top	Sample 1
BB_02	Barbados	UK FCDO	Worthing – house in south of island	13.0752836,−59.5851505	12 April 2021	12 April 2021	Dry sample of fallout between 06:00–11:00 from 25 × 25 cm glass table top	Sample 4

Samples SV_02–SV_12 may have been rained on prior to collection. U, stratigraphic unit from which samples SV_06–SV_12 were collected, from the deposit on a table at Richmond Vale Academy (Section 3 in Fig. 2, Cole *et al.* 2023). Thicknesses of SV_06–SV_12 refer to the total thickness of the unit rather than the sub-layer sampled. AC, accretionary lapilli present in the sample.
Sample collection: *UWI SRC (University of the West Indies Seismic Research Centre) – Richard Robertson; [†]UEA (University of East Anglia, UK) – Jenni Barclay; [‡]Plymouth (University of Plymouth, UK) – Paul Cole; [§]JT – Jenny Trumble; [¶]UK FCDO (UK Foreign, Commonwealth and Development Office) – Jonathan Stone.

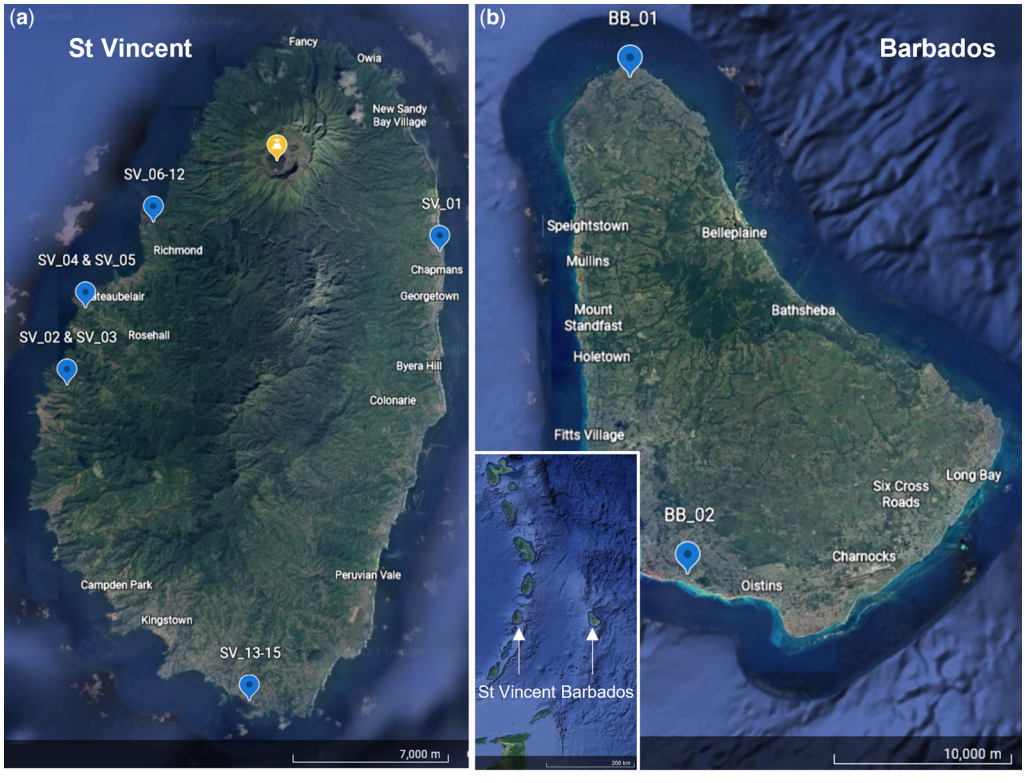

Fig. 2. Map of (**a**) St Vincent and (**b**) Barbados, showing locations of collected ash samples (blue placemarks) and La Soufrière volcano (yellow placemark). Inset shows the geographical locations of St Vincent and Barbados in the Eastern Caribbean, with a scale bar of 200 km. Source: map credit – Google Earth Version 9.181.0.1 (14 December 2015) https://earth.google.com, data – SIO, NOAA, US Navy, NGA, GEBCO CNES/Airbus Landsat, Copernicus, Mazar Technologies, LDEO-Columbia.

Richmond Vale Academy, St Vincent, on 26 April (Fig. 2). These samples were part of a campaign to collect tephra from deposits >4 km from the Summit Crater between 25 April and 10 May 2021 (Cole *et al.* 2023). Several units, composed of sub-layers, were identified by Cole *et al.* (2023) within the deposits and these were named U1 to U7 from the base upwards and could be correlated in deposits across the island (Table 1). A detailed description of the units is given in Cole *et al.* (2023). Samples for this study were obtained from within U1–U6.

Rainfall was recorded on St Vincent on 11 and 20 April during the explosive sequence, with further rainfall recorded locally on 27, 28 and 29 April prior to sampling (Phillips *et al.* 2023). Samples were collected from comparatively drier sites on St Vincent, where the ash was less affected by later precipitation.

The ash was sent to the UK where it was prepared (in DU and University of East Anglia (UEA) laboratories) by weighing the samples and drying them overnight in an oven at 70°C (except samples for leachate analyses, which were sub-sampled prior to drying). The dried samples were then sieved to >2, 1–2 and <1 mm and each fraction weighed. The <1 mm fraction was then used for all analyses except leachates. This is to prevent damage to the laser diffraction granulometer used to determine particle size distribution and aligns with previous implementations of the IVHHN protocol. Each ash sample (<1 mm size fraction) was mixed well, and then sub-samples of ash were extracted for each analysis.

Particle size measurements were conducted on all ash samples received (see Phase 2 of the IVHHN protocol, Fig. 1). Samples SV_01–05 and BB_01 and BB_02 were used for the Phase 3 analyses (samples SV_06–SV_15 were analysed for particle size separately). A summary of the analyses conducted on each ash sample is given in Table 2 and a map of sample locations where ash was collected is given in Figure 2.

Table 2. *Summary of analyses*

Ash sample #	Particle size	Crystalline silica	Morphology	Leachates	Bulk composition
SV_01	X	X	X	X	X
SV_02-05	X	X			X
SV_06-15	X				
BB_01-02	X	X	X	(X)	X

The leachate analyses in brackets were only conducted for assessment of contamination of water sources and ingestion hazards for livestock.

Crystalline silica identification and estimation in dome rock

SEM imaging with Energy Dispersive X-ray Spectroscopy (EDS) analyses were conducted at UEA (Zeiss Gemini 300 field emission SEM with Oxford Instruments Ultim Max 170 EDS detector) on five thin sections from 2020–21 (SVG-2021/16-1 through 5) plus the 1979 thin section, and at DU (Zeiss EVO 10 SEM with Zeiss SmartEDX) on one thin section from 2020–21. Imaging and analysis were conducted at 10 kV (UEA) or 15 kV (DU) with a working distance of 8.5 mm. The sections were screened for areas of glass devitrification and for evidence of vapour-phase crystal growth within vesicles and cracks, based on previous petrographic work by the authors (e.g. Damby 2012; Horwell *et al.* 2013*a*; Plail *et al.* 2014). When potential cristobalite patches were identified, spot EDS analyses were conducted, to confirm mineralogy. Crystalline silica (chemical composition SiO_2) is identified by an EDS spectrum containing Si and O. Volcanic cristobalite is distinguishable from quartz by small peaks of Al and Na in the EDS spectrum, due to impurities in the cristobalite crystal structure (Horwell *et al.* 2012).

After the thin sections had been reviewed, an estimate was made of the percentage cristobalite content in the dome rock by calculating the area of cristobalite in two 5 × 5 mm squares, containing representative proportions of glass devitrification, in images from the thin section with best resolution and contrast (SVG-2021/16-5). Devitrified regions were outlined manually and assigned a colour in the image processing software ImageJ. The thresholding tool was then used to calculate the area % of each image occupied by these regions. Crystalline silica content was then estimated with the assumption (based on careful observation of devitrified regions in all thin sections) that around 40–50% of the devitrified areas were glass and microlites.

Crystalline silica quantification in ash

XRD data were collected using an Enraf-Nonius PDS120 diffractometer equipped with a primary germanium (111) monochromator and an INEL 120° curved position sensitive detector (PSD) at the Natural History Museum, London. The operation conditions of the copper X-ray tube were 40 kV and 30 mA. The X-ray beam was collimated to 0.24 × 2 mm and the samples were analysed in asymmetric reflection geometry at a fixed tube–sample–detector arrangement. The angular linearity of the PSD was calibrated using the standards silver behenate and silicon.

Mineral quantification was performed using the Internal Attenuation Standard method of Le Blond *et al.* (2009). Ash samples were ground and mixed with 20 wt% zinc oxide (ZnO; the internal attenuation standard), and about 50 mg of sample was loaded in a small deep well holder for the measurements. Mineral standards of cristobalite (DKSmith), feldspar (labradorite, BM1926, 1522), pyroxene (augite, Bohemia) and synthetic zinc oxide (ZnO) were analysed using the same XRD conditions. The data collection time was 1 h for samples and 20 min for standards.

The mass attenuation coefficient for St Vincent ash composition was determined for sample BB_01 and used for all sample quantifications. DKSmith cristobalite is a well-crystallized, high-purity standard, with greater diffraction intensities than volcanic cristobalite (Damby *et al.* 2014), and use of which results in cristobalite quantifications for volcanic ash that can be considered minimum values.

Particle size distribution

Samples were analysed on a Beckman Coulter LS13 320 Particle Size Analyser (laser diffraction granulometer) at DU using an optical model applying Mie theory to raw data (using a refractive index of 1.33 for water, 1.60 for the ash (based on the basaltic andesite magma type; Horwell 2007) and an absorption coefficient of 0.1) and Polarization Intensity Differential Scattering (PIDS) technology. Each sample was introduced to a fluid module, containing water, until nominal obscuration and PIDS values (of about 10% obscuration and 60% PIDS) were achieved. Sonication was applied for 20 s and a wait time of 10 s prior to data acquisition, where

run time was 90 s and 3 runs were performed. The mean of these 3 runs was produced to yield the data (both raw and cumulative). As volcanic ash is defined as particles <2 mm diameter, a calculation was then performed to add in the mass of the 1–2 mm fraction which was not introduced to the instrument. This only applied to the St Vincent samples SV_01, 06–09 and 12, as none of the other samples contained particles >1 mm diameter. See Supplementary material for detail.

Particle morphology

Ash from samples SV_01, BB_01 and BB_02 was sprinkled onto polycarbonate discs which were stuck to carbon sticky pads on aluminium SEM stubs, using a dry cotton bud. Samples SV_01 and BB_01 were chosen because they represented the earliest phases of the explosive eruptions, when the domes (which were likely to be hydrothermally altered) were destroyed. Sample BB_02 was chosen for comparison. The stubs were coated with gold-palladium to prevent charging of particles. SEM-EDS analyses were conducted at DU (Zeiss EVO 10 SEM with Zeiss SmartEDX and Hitachi SU-70 field emission SEM with Oxford Instruments X-Max^N 50 mm^2 Silicon Drift Detector) on the three ash samples. Imaging and analysis were conducted at 15 kV, with working distances of 11.5 mm on the Zeiss and 15 mm on the Hitachi SEM. Images of fibres were taken on the Zeiss instrument and images of the broader ash morphology were taken on the Hitachi instrument. When fibre-like particles (aspect ratio of >3:1; World Health Organization 1997) were visually observed, EDS spot analyses were conducted to identify the composition of the particles.

Bulk composition of ash

Major element data were obtained by XRF analysis using a Panalytical Axios Advanced WD-XRF spectrometer at the University of Leicester, UK. Major elements were determined on fused glass beads, composed of dry sample material and 100% lithium tetraborate flux in a 1:30 ratio (0.2 g sample, 6 g flux) with results quoted as component oxide weight percent recalculated to include total loss on ignition (LOI) in the final total, in order to eliminate mineralogical effects and reduce inter-element effects. LOI was measured on pre-dried powders after ignition at 950°C in air for 90 minutes. Instrumental conditions were selected to avoid any significant line overlaps within the usual compositional range of most geological materials. Suitable drift monitoring samples were analysed at the commencement of each analytical run and calibrations were set using international rock reference materials under the same conditions and regressing the measured count ratios against the recommended concentrations, principally from Govindaraju (1994) and values published on the GeoREM reference site (http://georem.mpch-mainz.gwdg.de/), utilizing Panalytical's fundamental parameters correction software.

Leachate analyses for ash respiratory hazard

Ideally, the risk of PTEs leaching into the lungs from ash surfaces would be assessed using simulated lung fluid (SLF) as the leachant. However, the reagents required may not be available in laboratories responding to eruption crises and some of the elements of interest may not be reliably quantified due to matrix effects (i.e. the leachant also contains those elements) (Stewart *et al.* 2020; Tomašek *et al.* 2021). Tomašek *et al.* (2021) showed that a standard deionized water leach could be used as a conservative proxy for SLF. They also found that PTE concentrations reach steady-state dissolution by 24 hours of leaching. Therefore, ash sample SV_01 was leached for 24 hours using deionized water, at a ratio of 1 g ash to 100 ml extractant at the US Geological Survey (Menlo Park, CA), following the IVHHN leachate protocol for respiratory exposures (Stewart *et al.* 2020). Note that only sample SV_01 was analysed for respiratory hazard assessment due to the low quantity of ash received for the Barbados samples and because samples SV_02–SV_05 were likely rained on prior to collection (samples SV_06–SV_15 were not available as part of the Phase 3 analyses; Table 2). Concentrations of leached anions and cations were quantified using ion chromatography (IC; Dionex ICS-2000) and inductively coupled plasma optical emission spectrometry (ICP-OES; Thermo Scientific iCAP 6000), respectively. The pH of the leachates were also measured. Leachate data are presented as milligrams of the leachable element per kilogram of ash (mg kg^{-1}) on a dry weight basis. Sample data are blank-subtracted as applicable and data rounded to reflect precision.

Leachate analyses to assess contamination of water resources and ingestion hazards for livestock

Deionized water leaches can be used to assess the release of readily water-soluble compounds on ash particle surfaces and are applicable for purposes such as predicting composition changes in water sources used for water supplies and roof catchment rainwater tanks, and the addition of plant growth nutrients for immediate uptake by crops. A simple gastric leach estimates the bioaccessible fraction (the fraction that is soluble in biological conditions) of toxicants to livestock from ingested (eaten) ash.

Leachate experiments, on pristine ash samples SV_01, BB_01 and BB_02, followed the procedures described in an internationally ratified protocol for volcanic ash (Stewart *et al.* 2020 and https://www.ivhhn.org/uploads/IVHHN%20leachate%20protocol.pdf). Water leaches were performed at ash to leachant ratios (g:ml) of 1:20 and 1:100, as per recommendations in the protocol, in deionized water for 1 hour. These two complementary ratios are recommended as, at the 1:100 ratio, some elements may be below detection limits and, at the 1:20 ratio, dissolution of some compounds may be incomplete due to saturation effects. The gastric leach was performed at 1:100 in 0.032 M hydrochloric acid (HCl, pH 1.5). Sample SV_01 was run in duplicate as part of data quality management. The pH was measured, and concentrations of leached anions and cations were quantified (IC and ICP-OES), respectively. Leachate data are presented as milligrams of the leachable component per kilogram of ash (mg kg^{-1}) on a dry weight basis.

Results and discussion

Bulk composition

XRF analyses confirmed that the ash samples acquired for this study can all be classified as basaltic andesite in composition, with bulk SiO_2 contents of 52.3–53.8 wt% and $K_2O + Na_2O$ contents of 4.0–4.6 wt% as shown in the total alkali v. silica plot (Le Bas and Streckeisen 1991) in Figure 3. The raw data are given in Table 3. Visually, the magmatic composition of the ash samples is slightly more mafic (SiO_2-poor) than the composition of 2021 dome and explosive scoria samples reported by Joseph *et al.* (2022), which had 54–56 wt% SiO_2. This is consistent with slight winnowing of glass shards with transport (Horwell *et al.* 2001).

Crystalline silica identification and estimation in dome rock

We identified less than 2 area % crystalline silica in the 2020–21 dome rock and no crystalline silica in the 1979 dome rock thin sections. This suggested that there was a low probability that the subsequent explosion ash would contain substantial quantities of this phase.

It is noted, however, that the 1979 sample was retrieved within weeks of extrusion onset, so it is unknown to what extent the dome crystallized during the rest of the 1979 eruption and since that time. It should also be noted that the 2020–21 dome rock was collected around three weeks after dome growth began and from the surface of the dome. Therefore, this dome rock may not be representative of the

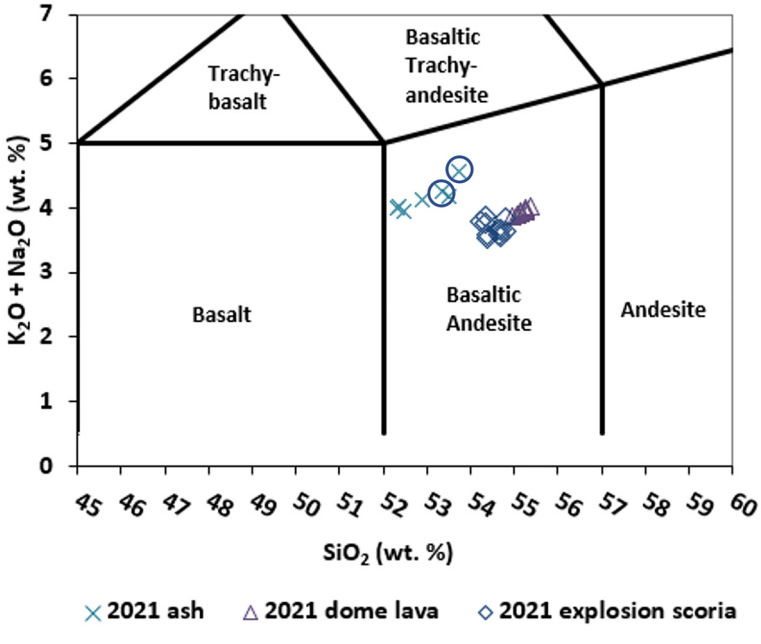

Fig. 3. Total alkali v. silica plot from XRF data of 2021 ash samples SV_01–SV_05 and BB_01 & 02 (symbols within circles), with data from Joseph *et al.* (2022) from samples of 2021 dome lava and explosion scoria. Raw data are presented in Table 2.

Table 3. *X-ray fluorescence data of major elements determined on fused glass beads prepared from dried powders*

Sample	SiO_2	TiO_2	Al_2O_3	Fe_2O_3	MnO	MgO	CaO	Na_2O	K_2O	P_2O_5	SO_3	LOI	Total
BB-01	53.75	0.90	19.62	8.24	0.17	3.56	8.62	3.99	0.57	0.13	0.03	0.22	99.81
BB-02	53.36	0.92	19.60	8.21	0.17	3.49	8.64	3.70	0.55	0.13	<0.006	0.35	99.11
SV-01	52.38	0.94	19.08	8.87	0.18	4.24	9.02	3.51	0.51	0.12	0.03	0.05	98.94
SV-02	52.90	0.92	19.65	8.35	0.17	3.77	8.96	3.61	0.52	0.12	0.05	0.20	99.23
SV-03	52.48	0.94	19.60	8.78	0.18	4.15	9.18	3.46	0.49	0.12	0.04	0.05	99.46
SV-04	52.33	0.97	19.12	9.03	0.19	4.22	8.99	3.49	0.50	0.12	0.06	0.68	99.71
SV-05	53.51	0.91	19.67	8.27	0.17	3.75	8.89	3.66	0.53	0.13	0.23	0.41	100.14

Results quoted as component oxide weight percent re-calculated to include loss on ignition (LOI) in final total.

average dome composition or cristobalite abundance and, consequently, hazard. At the time of sampling, growth of the dome was exogenous. The dome grew laterally, primarily, giving a large surface area that would facilitate cooling of the material. In the last few days of the dome-forming phase of the eruption, there was rapid inflation of the dome (Stinton 2023). The surface temperature of the dome was measured to be around 600°C (Joseph *et al.* 2022), suggesting that the interior of the dome would have cooled sufficiently slowly to allow for cristobalite to form and persist metastably (i.e. outside of its stability field, <200 MPa pressure and *c.* 1470–1727°C (Heaney 1994)). The inclusion of aluminium and sodium in its crystalline structure may allow volcanic cristobalite to form at temperatures that are far below the cristobalite stability field (Damby 2012; Damby *et al.* 2014). Morrison-Evans *et al.* (2023) suggest that the breakdown of clinopyroxene rims, and the existence of devitrification patches, may be the result of high-temperature oxidation at, or close to, the dome surface. There is some evidence to suggest that the 2020–21 magma could have resided at shallow depths as a remnant from the 1979 eruption (Weber *et al.* 2023). If this is the case, the devitrification may have occurred over the past 40 years rather than in the three weeks following dome emplacement.

The 2020–21 thin sections showed patches of devitrification, which were typically restricted to regions adjacent to larger oxides. These patches are identified as areas of dark grey groundmass (compared to lighter grey, unaltered groundmass), where cristobalite has replaced glass and sometimes has a symplectic (interwoven) texture with glass or plagioclase feldspar (see Fig. 4a, b). EDS spot analysis of dark grey patches in extensively devitrified areas confirmed these areas as cristobalite (O, Si>>Al>Na, in order of elemental abundance). Some devitrification was also associated with breakdown of the rims of clinopyroxene phenocrysts (large crystals). In these areas, which sometimes showed evidence of corrosion (holes in microlites and groundmass, and complete breakdown of some

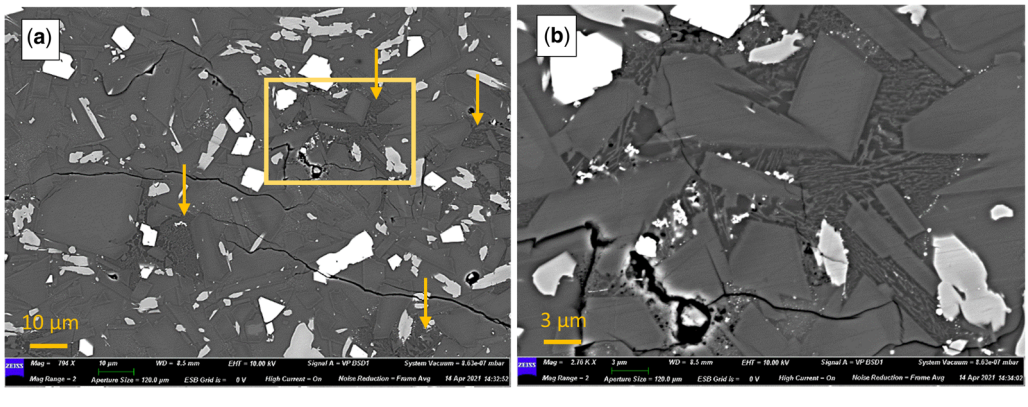

Fig. 4. Backscatter scanning electron microscopy images of thin sections from dome rock sample SVG-2021/16 showing devitrification textures. (**a**) Image shows several patches of devitrification (dark grey groundmass; indicated by yellow arrows). (**b**) Higher magnification of the area in the yellow box in (a), showing detail of devitrification texture. The dark grey is cristobalite and the lighter grey 'interwoven' texture is plagioclase feldspar or glass, among larger, lighter grey feldspar microlites, and iron oxides (light grey/white).

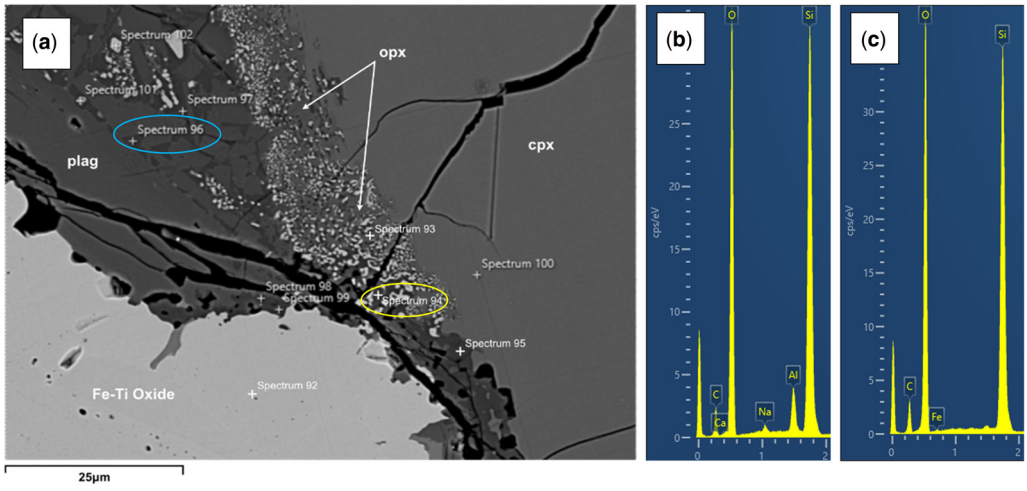

Fig. 5. (**a**) Backscatter scanning electron microscopy image from thin section sample SVG-2021/16 showing oxide (bright dots) and clinopyroxene breakdown textures. cpx, clinopyroxene; opx, orthopyroxene; plag, plagioclase feldspar. (**b**) EDS spectrum for spot 96 showing typical cristobalite peaks (O, Si>>Al>Na). (**c**) EDS spectrum for spot 94 showing a quartz spectrum (O, Si). C peaks are from the carbon coating on the thin section. The spot locations and labels are shown by a + sign and yellow (spot 94) and blue (spot 96) ovals.

groundmass areas, Fig. 5a), there may be a mixture of quartz (O, Si) and cristobalite (Fig. 5), based on similar textures observed and analysed in previous studies (e.g. Horwell *et al.* 2013*b*). No evidence of vapour-phase cristobalite was identified. Such crystals would be clearly observed protruding from the walls of vesicles and cracks, typically displaying characteristic fish-scale cracking in thin section, with a hexagonal or fan-like morphology (Damby 2012; Horwell *et al.* 2013*a*). Instead, vesicles were often lined with clinopyroxene crystals, perhaps indicating that any circulating vapours in the dome were less silica-rich than those capable of precipitating cristobalite.

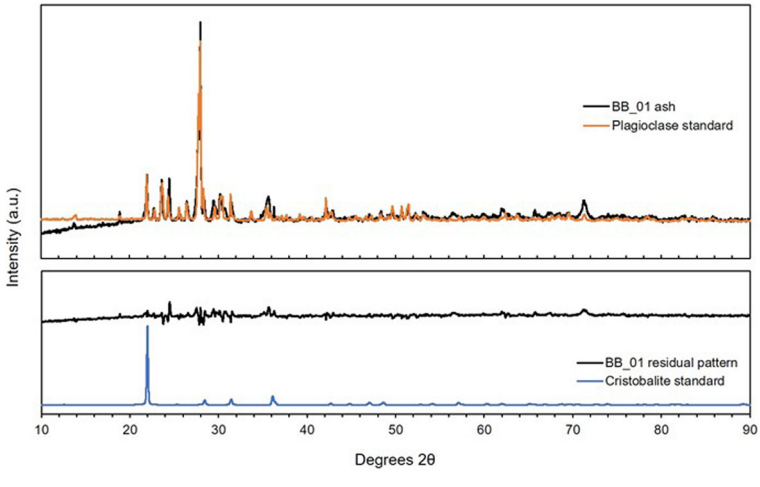

Fig. 6. Representative X-ray diffraction pattern of St Vincent ash. The top patterns present an overlay of ash sample BB_01 (black) with a plagioclase feldspar standard (labradorite; orange), showing a close match between patterns. The bottom patterns display the residual BB_01 ash pattern (black) after the plagioclase component has been stripped out, with the cristobalite standard (blue) to identify the presence of cristobalite. Pattern intensity is presented in arbitrary units (a.u.).

Table 4. *Particle size results in cumulative vol% for the key respiratory health-pertinent size fractions*

Size fraction (<μm)	1	2.5	4	10	100	Date erupted
SV_01	2.4	5.3	7.3	13.7	48.8	9–10 April 2021
SV_02	3.1	6.6	9.0	15.9	74.5	*c.* 9–11 April 2021
SV_03	2.6	5.8	7.9	14.0	50.9	*c.* 11–22 April 2021
SV_04	2.8	6.4	9.0	17.2	53.5	*c.* 9–11 April 2021
SV_05	3.7	7.8	10.6	19.6	81.3	*c.* 11–22 April 2021
SV_06	2.4	5.9	4.0	15.2	48.2	10–11 April 2021
SV_07	2.1	5.4	8.3	14.6	40.0	10–11 April 2021
SV_08	2.1	5.1	7.7	14.1	38.9	10–11 April 2021
SV_09	2.0	5.3	7.3	15.4	34.0	10–11 April 2021
SV_10	3.2	6.9	7.7	18.2	64.0	10 April 2021
SV_11	3.1	7.3	10.4	20.7	68.4	10 April 2021
SV_12	0.9	2.4	3.7	7.0	12.5	9–10 April 2021
SV_13	3.5	7.5	10.2	18.6	92.8	10 April 2021
SV_14	3.9	7.9	10.7	19.4	96.6	10 April 2021
SV_15	3.4	7.7	10.6	19.1	96.0	10 April 2021
BB_01	3.3	7.4	10.4	19.8	69.0	9–10 April 2021
BB_02	2.8	5.7	7.7	14.8	68.3	12 April 2021

Crystalline silica quantification in ash

Figure 6 is a representative XRD pattern (sample BB_01). Quantitative evaluation revealed the presence of plagioclase feldspar and an amorphous phase (glass) as the two dominant phases, with trace pyroxene present. Low amounts of cristobalite were identified in all ash samples (<5 wt%) and there was no systematic difference between the samples deposited during the phase when the domes were destroyed (9–11 April) and the later samples. However, samples SV_02 (the first few mm of ash deposited during the eruption) and BB_01 (a distal bulk sample of ashfall also from 9 to 10 April) contained more cristobalite than other samples, and detailed mineralogical analysis of the deposit stratigraphy may reveal a clearer relationship with incorporated dome (cristobalite-bearing) material. As would be expected, little to no quartz was apparent in the ash samples by XRD.

To compare this result with other volcanoes (and analyses using the same XRD quantification technique), Damby (2012) showed that dome rock of different magmatic compositions contains between 0 and 24 wt% cristobalite, with higher bulk SiO_2 correlating with increased cristobalite abundances. Consistent with this finding, the amount of crystalline silica in La Soufrière ash is much less than that measured in andesitic dome collapse ash from nearby Soufrière Hills volcano, Montserrat, which had up to 23 wt% cristobalite, and 3–18 wt% in ash generated from explosions and ash venting through the existing dome (Horwell *et al.* 2014).

Large quantities of crystalline silica would not be expected in young basaltic andesite lavas due to insufficient quantities of SiO_2 in the melt/glass, unless it had already undergone substantial groundmass crystallization. In the explosive eruptions, the pulverized dome rock will also have been 'diluted' with ash derived from juvenile magma. Le Blond *et al.* (2010) found 2.4 wt% cristobalite in a sample of basaltic andesite ash from Langila volcano, Papua New Guinea, erupted in 2007. It is not established if there was dome material present in the crater prior to the eruption. Damby *et al.* (2013) analysed basaltic trachy-andesitic ash (containing more Na_2O and K_2O than basaltic andesitic ash but similar quantities of bulk SiO_2) from the 2010 Merapi eruption where, like at La Soufrière, both juvenile and older dome material were incorporated in explosive events (Surono *et al.* 2012). The Merapi ash contained between 1.9 and 9.5 wt% cristobalite, which is raised in comparison to ash of similar magmatic composition but with no dome incorporation (e.g. the 2010 Eyjafjallajökull eruption contained <2 wt % cristobalite) (Horwell *et al.* 2013*b*).

Particle size distribution

Table 4 shows the cumulative quantity of material (in vol%) less than each of the particle size thresholds given. These are roughly comparable to PM1, 2.5, 4, 10, 100, which are the particulate matter (PM) fractions of respiratory importance (see Introduction). The amount of respirable (<4 μm or <2.5 μm) and thoracic (<10 μm) material in the ash is typical of highly explosive eruptions (Horwell 2007) – in other words, there is a substantial fraction of ash that can be inhaled into the lungs, in most

samples, regardless of when they were erupted or where they were sampled. An exception to this is SV_12 from U1 which, as also noted by Cole *et al.* (2023), is notably coarse-grained with only 12.5 vol% sub-100 μm material and 7 vol% sub-10 μm material compared with 20.7 vol% for SV_11 which comes from U2, deposited a few hours later. U1 represents the initial explosion, which occurred at 12:41 UTC on 9 April and was followed by smaller, near-continuous pulsatory eruptions with plumes that dispersed to the ENE (Cole *et al.* 2023). The initial explosion produced lapilli-sized tephra which formed as the 2020–21 and 1979 domes were fragmented (Cole *et al.* 2023).

Samples SV_06–SV_08 contained accretionary lapilli. Cole *et al.* (2023) hypothesize that the accretionary lapilli were formed when pyroclastic density currents (PDCs) entered the ocean; they are only present in U3 to U7 on the western side of the island (the same side as the valleys where PDCs travelled), and coincide with PDC generation in the chronology of the eruption, but there was also precipitation at times (from 11 April onwards), which may also have contributed to the ash aggregation. Therefore, these ash layers could have resulted either from elutriation of ash from the PDCs or directly from the explosion plume (Cole *et al.* 2023). Although the ash was sampled with accretionary lapilli intact, and these remained intact post-transport and sieving to <1 mm, it is likely that the accretionary lapilli disaggregated during particle size analysis, with the use of sonication. This is assumed because sample SV_08 is from the same unit (and location) as SV_09 (U3) but had accretionary lapilli in it originally, yet the measured particle size distributions are very similar. Additionally, we lightly crushed one sample (SV_08), after sieving to 1 mm, to disaggregate the accretionary lapilli and the data for the crushed and uncrushed samples are identical (data for crushed sample not shown).

SV_13–SV_15 were collected from the south of St Vincent, around 20 km from the volcano. They are notable because almost 100 vol% of the samples, collected over the first *c.* 24 hours of the eruption, are sub-100 μm in diameter and almost 20 vol% of the samples are sub-10 μm. This likely reflects the distance from the volcano but this does not fully explain the fineness of these samples given that BB_01, collected on Barbados in the same timeframe (and with a very similar distribution in the fractions up to 10 μm), only has 69 vol% sub-100 μm material.

Particle morphology

SEM imaging (Figs 7 & 8) showed that the thoracic fraction (<10 μm diameter) ash particles were angular and blocky, with finer (<2.5 μm) particles often adhered to larger particles. This morphology is typical of ash particles of this size (e.g. Le Blond *et al.* 2010; Horwell *et al.* 2010*b*, 2013*a*; Damby *et al.* 2013; Eychenne *et al.* 2022). Sparse (estimated at <0.01 num%), fibre-like particles were observed, especially in SV_01 and BB_01, from the initial explosions on 9–10 April, which

Fig. 7. Scanning electron microscopy image (Hitachi SEM) of sample SV_01 showing that the thoracic fraction (<10 μm) ash particles are mostly blocky and angular in shape, with smaller particles adhering to larger ones. Scale bar is 25 μm.

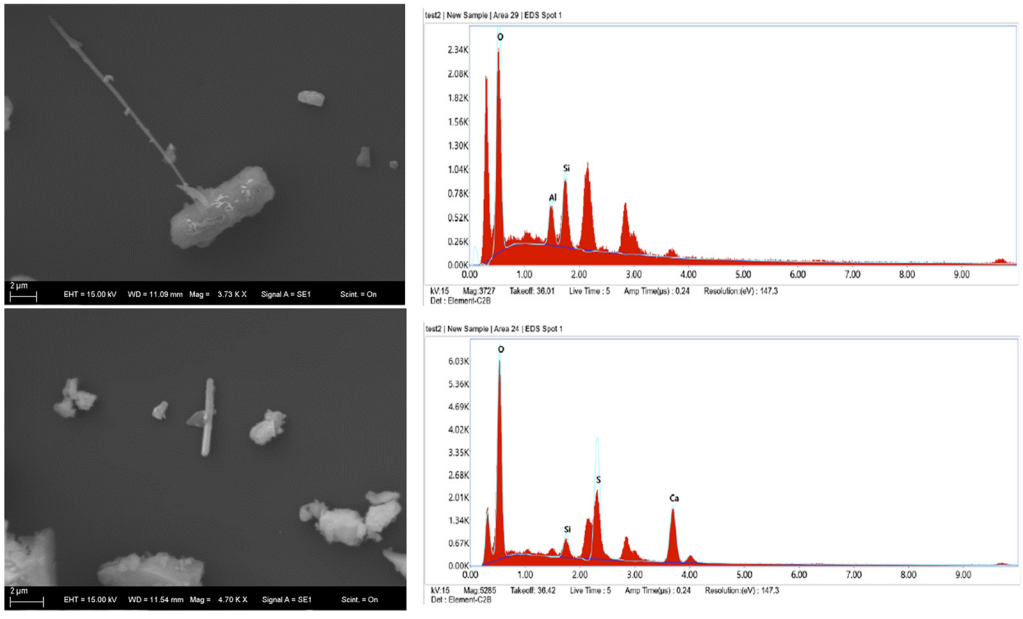

Fig. 8. Scanning electron microscopy images (Zeiss EVO SEM) showing examples of fibre-like particles with associated EDS spot analysis spectra. Top left image shows a very high aspect ratio particle lodged against a 'stubby' particle. EDS analysis of the fibre-like particle (top right) showed that the particle was made primarily of Si + Al with ratios typical of plagioclase feldspar (minor peaks of Na + Ca not labelled). The lower left image shows a small fibre-like particle which EDS analysis found to be composed of S + Ca (lower right), indicative of gypsum or anhydrite (both $CaSO_4$). Note that most unlabelled peaks are the gold-palladium coating added to the SEM stub. Scale bars of both images are 2 μm.

we confirmed to be primarily calcium sulfate ($CaSO_4$; gypsum or anhydrite), with occasional plagioclase feldspar and an Fe/Mg silicate (possibly pyroxene) which does not appear to be related to asbestos (Fig. 8). Ash-associated calcium sulfate is lung-soluble and minimally reactive i*n vitro*, and not considered to be a respiratory hazard (Tomašek *et al.* 2019).

Cole *et al.* (2023) confirmed that some ash (up to 20 wt%) from the initial explosions (seen in U1 deposits) was generated from hydrothermally altered deposits, which they suggest were from the 1979 lava dome. Ball *et al.* (2015) showed that persistent heat and high permeabilities are required to cause alteration and that it usually occurs at the core/talus interface. Therefore, if the $CaSO_4$ observed in ash was dome derived, it would likely be from the 1979 lava as there was insufficient time for extensive alteration of the 2020–21 dome. $CaSO_4$ can also be formed through within-plume ash-gas reactions where sulfate salts form on the surface of ash particles (Ayris *et al.* 2013) and by scavenging of sulfur dioxide by fragmented particles in fracture networks within (at least rhyolitic) domes (Casas *et al.* 2019). Work is in progress to differentiate sources of $CaSO_4$ in ash using sulfur isotopes (e.g. King *et al.* 2023) but, for now, the source of such particles cannot be confirmed.

Leachate analyses for ash inhalation hazard

Sample SV_01 had a slightly acidic pH of 5.53 (Table 5). Manganese was the most abundant trace

Table 5. *pH and water-extractable concentrations (after 24 h and at a ratio of 1:100) of potentially toxic elements for sample SV_01 (in mg kg^{-1} ash)*

	SV_01	2016 Whakaari	2018 Ambae	2018 Kīlauea
pH	5.53			
Al	3.79	3018	72.8	229.2
Cd	<0.1	0.08	0.02	0.04
Co	0.19	10.6	0.66	2.88
Cr	<0.1	4.2	bd	0.06
Fe	<0.06	818.6	4.0	1420
Mn	10	83.2	31.1	95.4
Ni	0.38	20.4	2.6	9.1
Zn	0.62	10.2	2.2	4.7

Comparative data from Tomašek *et al.* (2021) using the same methods for three recent eruptions are shown alongside. bd, below detection limit.

metal mobilized upon exposure to water. Water-extractable concentrations in sample SV_01 are low to very low in comparison to ash from the 2016 eruption of Whakaari/White Island volcano, New Zealand, the 2018 eruption of Ambae volcano, Vanuatu, and the 2018 eruption of Kīlauea volcano, Hawaii (Tomašek *et al.* 2021) determined using the same method (24-hour leach, 1:100 ratio). From a respiratory health hazard perspective, the concentrations of the PTEs in SV_01 presented in Table 4 are unlikely to be of concern.

Leachate analyses to assess contamination of water sources and ingestion hazards for livestock

Water-extractable elements are shown in Table 6, with global median data (Ayris and Delmelle 2012) shown alongside for comparison. For most elements, similar, although slightly higher, concentrations were reported in the 1:100 v. the 1:20 leaches. For aluminium, bromine and silicon (as SiO_2), consistently higher concentrations were reported for 1:100 leaches than 1:20 across all samples, indicating inhibited dissolution at the 1:20 ratio. Concentrations are generally low in comparison to global median values, with exceptions being barium (for sample SV_01) and bromine (for samples BB_01 and BB_02).

Concentrations of elements extracted by the gastric leach are also shown in Table 6. As expected, the gastric leach extracted greater quantities of almost all elements in all samples. The most dramatic increases were for aluminium, iron, phosphate and silicon (as SiO_2), consistent with observations from other eruptions (Cronin *et al.* 2014; Stewart *et al.* 2020). More modest increases in the concentrations of PTEs cobalt, chromium, fluoride, manganese and nickel were observed. In general, physical effects of ash

Table 6. *pH, water- and HCl-extractable (gastric leach) elements (in mg kg^{-1} ash) for samples SV_01, BB_01 and BB_02*

	SV_01	BB_01	BB_02	SV_01	BB_01	BB_02	SV_01	BB_01	BB_02	Global median concentrations (in water)
Ratio	**1:20**	**1:20**	**1:20**	**1:100**	**1:100**	**1:100**	**1:100**	**1:100**	**1:100**	
Leachant	**Water**	**Water**	**Water**	**Water**	**Water**	**Water**	**HCl**	**HCl**	**HCl**	
pH	5.71	5.72	5.83	5.75	5.44	5.44				
Al	0.05	1.9	0.92	0.34	7.2	1.92	548	543	525	58
As	<0.02	0.07	0.04	0.03	0.06	0.02	<0.1	<0.1	<0.1	0.13
B	<0.2	<0.4	<0.6	<1	<1.01	<1.01	<0.99	<1.01	<1.01	2.6
Ba	2.75	<0.4	<0.06	8.8	<0	<0.1	1.34	1.57	1.2	0.94
Br	<1	2.6	3.8	<5	6.1	9.1	<4	<5	<4	1.9
Ca	370	524	59	398	562	80	1200	1440	820	2140
Cd	<0.02	<0.04	<0.06	<0.1	<0.1	<0.1	<0.1	<0.1	<0.1	0.053
Cl	460	430	55	470	440	65	n/a	n/a	n/a	1162
Co	0.11	0.07	<0.06	0.14	<0.1	<0.1	0.26	0.21	0.11	0.186
Cr	<0.02	<0.04	<0.06	<0.1	<0.1	<0.1	0.28	0.25	0.29	0.096
F	12	23	4.0	17	26	4.1	25	32	15	129
Fe	<0.06	<0.12	0.53	<0.3	<0.3	0.48	207	172	212	21
K	24	26	4.6	12	22	4.8	77	89	87	71
Li	0.14	0.11	0.09	<0.1	<0.1	<0.1	0.19	0.17	<0.1	0.22
Mg	77	70	13	82	74	17	166	161	124	335
Mn	8.3	7.2	1.1	8.9	8.1	1.8	16	17	10	20
Mo	<0.02	<0.04	<0.06	<0.1	<0.1	<0.1	<0.1	<0.1	<0.1	0.063
Na	161	146	9	147	77	<20	254	262	121	378
Ni	0.19	0.13	<0.06	0.23	0.19	0.1	0.47	1.6	0.47	0.50
NO_3	<1	2.4	<1	<5	<5	<5	<4	<5	<4	22
PO_4	<1	<1	<1	<5	<5	<5	170	190	190	227
Rb	<0.2	<0.4	<0.6	<1	<1.01	<1.01	<0.99	<1.01	<1.01	0.083
Se	<0.1	<0.2	<0.3	<0.5	<0.51	<0.51	<0.5	<0.51	<0.5	0.055
SiO_2	9.1	7.8	16	25	24	29	1230	1240	1160	54
SO_4	920	1180	130	950	1190	88	1560	1860	400	4986
Sr	0.69	1.02	0.05	0.72	0.89	<0.1	2.3	2.9	1.7	4.3
Zn	2.1	<0.04	<0.06	7.5	<0.1	<0.1	1.7	5.6	5.6	3.6

All data are from 1-hour extractions.
Global median data are from Ayris and Delmelle (2012) and represent analyses conducted at a range of leachate ratios.

ingestion by livestock dominate over toxicological impacts from elements leached from ash surfaces (see Supplementary material). Poisoning is associated primarily with high fluoride in ash and, in some cases, very high concentrations of sulfur. Very rarely, problems may arise from high concentrations of copper or zinc. For the 2021 La Soufrière ash samples, bioaccessible concentrations of fluoride, sulfur (as sulfate) and zinc are low in comparison with ash from other recent eruptions (Stewart *et al.* 2020). As animals would have to ingest large quantities of ash to reach toxicological thresholds, it is likely that they would suffer physical problems such as tooth abrasion, irritant effects and intestinal blockages before any toxicological impacts would manifest.

It should be noted that these analyses were only conducted on three samples: one sample from St Vincent and two from Barbados. While there is good consistency in data among samples, these findings may not be fully representative of the ash that fell across the islands.

Outcomes and conclusions

When compared to ash analysed from other eruptions, the La Soufrière 2021 ash is considered to have sufficient material to be of respiratory concern (i.e. there was substantial ash in the environment that was fine enough to be inhaled into the lung, and particularly the alveolar region). The presence of crystalline silica as cristobalite in the incipient 2020–21 dome rock (<2 area %) warranted consideration of an airborne crystalline silica hazard; however, the minimal crystalline silica in the ash (<5 wt %) considerably reduces concern related to respirable crystalline silica exposure risk. It is also reassuring that there are few fibre-like particles in the ash, and none were analysed of a concerning composition. It should be noted that, whilst the particles are described as angular, particles of this size are not 'sharp' and will not lacerate the lungs. The low concentrations of lung-soluble potentially toxic elements are also reassuring. The generally low soluble salt cargo associated with these ash samples implies a low potential to contaminate water supplies or to harm livestock through ingestion. We note that local response efforts should also be informed by direct analysis of both raw water sources and treated drinking water (IVHHN 2021).

Therefore, the greatest hazard to respiratory health is the abundance of respirable particles in the ash. Such particles will continue to be remobilized into the air during dry periods, via clean-up activities, by vehicles, agricultural activities and wind, until such time as the ash is completely removed or reworked into the soil, which could take years to decades. The World Health Organization has concluded that both fine and coarse particulate matter (including crustal particulate) is capable of causing respiratory and cardiovascular mortality and morbidity associated with a wide range of health outcomes (World Health Organization 2013). Particulate matter has also been classed as carcinogenic (Loomis *et al.* 2013). Therefore, efforts to reduce exposures should be made, particularly for those individuals in vulnerable groups (e.g. children, older people, those with existing respiratory or cardiovascular conditions) or who work in outdoor occupations. As part of the IVHHN protocol, a report on the analyses presented here was submitted to the Pan American Health Organization (PAHO), the St Vincent and Grenadines Ministry of Health and the Caribbean Public Health Agency (CARPHA), which also outlined the value of monitoring personal exposure and airborne concentrations of particulate matter for assessment of health risk. This resulted in PAHO planning and implementing a low-cost particulate sensor network on the island, to monitor re-suspension of ash after the eruption ceased (Pan American Health Organization 2021).

Acknowledgements With thanks to Madeleine Humphreys (Durham University, UK), Shane Cronin (University of Auckland, New Zealand), Ines Tomašek (University of Clermont Auvergne, France) and Peter Baxter (University of Cambridge, UK) for reviewing the original reports which were presented to relevant agencies during the eruption crisis. Thanks to Richard Robertson (UWI SRU), Thomas Christopher (MVO), Jonathan Stone (UK FCDO), Paul Cole (University of Plymouth, UK), Jenny Trumble, and Madeleine Humphreys (Durham University, UK) for ash and dome rock sample collection and provision, and to David Pyle (Oxford University, UK) for provision of 1979 dome rock. Thanks also to Jesús Montes Rueda at the University of Granada and Ian Chaplin at Durham University for thin sectioning of dome rock samples and to the Durham University GJ Russell Electron Microscopy Facility. Thanks to Ed Llewellin for support with the PSD calculation and explanation. Any use of trade, firm, or product names is for descriptive purposes only and does not imply endorsement by the US Government.

The authors are very grateful to Natalia Deligne and Tom Sheldrake for their helpful reviews and to USGS reviewers.

Competing interests The authors declare that they have no known competing financial interests or personal relationships that could have appeared to influence the work reported in this paper.

Author contributions **CJH**: conceptualization (lead), data curation (lead), formal analysis (equal), funding acquisition (lead), investigation (lead), methodology (equal), project administration (lead), resources (lead), supervision (equal), validation (lead), visualization (lead), writing – original draft (lead), writing – review & editing

(lead); **DED**: conceptualization (supporting), data curation (equal), formal analysis (equal), investigation (equal), methodology (equal), supervision (equal), validation (equal), visualization (equal), writing – original draft (equal), writing – review & editing (equal); **CS**: investigation (supporting), methodology (supporting), validation (supporting), visualization (supporting), writing – original draft (supporting), writing – review & editing (supporting); **EPJ**: investigation (supporting), writing – original draft (supporting), writing – review & editing (supporting); **JB**: conceptualization (supporting), data curation (supporting), formal analysis (supporting), investigation (supporting), methodology (equal), supervision (equal), validation (equal), writing – original draft (equal), writing – review & editing (equal); **BVD**: formal analysis (equal), methodology (equal), visualization (equal), writing – original draft (supporting), writing – review & editing (supporting); **MFM**: formal analysis (supporting), methodology (supporting), visualization (supporting), writing – original draft (supporting), writing – review & editing (supporting); **LGM**: formal analysis (equal), methodology (equal), writing – original draft (supporting), writing – review & editing (supporting); **JN**: formal analysis (equal), methodology (equal), writing – original draft (supporting), writing – review & editing (supporting); **SP**: formal analysis (equal), methodology (supporting), writing – original draft (supporting), writing – review & editing (supporting); **NT**: formal analysis (equal), methodology (equal), writing – original draft (supporting), writing – review & editing (supporting).

Funding IVHHN protocol analyses were funded by the Pan American Health Organization. Jenni Barclay acknowledges a GCRF Cluster Grant.

Data availability All data generated or analysed during this study are included in this published article (and its supplementary information files).

References

Ayris, P.M. and Delmelle, P. 2012. The immediate environmental effects of tephra emission. *Bulletin of Volcanology*, **74**, 1905–1936, https://doi.org/10.1007/s00445-012-0654-5

Ayris, P.M., Lee, A.F., Wilson, K., Kueppers, U., Dingwell, D.B. and Delmelle, P. 2013. SO_2 sequestration in large volcanic eruptions: high-temperature scavenging by tephra. *Geochimica et Cosmochimica Acta*, **110**, 58–69, https://doi.org/10.1016/j.gca.2013.02.018

Ball, J.L., Stauffer, P.H., Calder, E.S. and Valentine, G.A. 2015. The hydrothermal alteration of cooling lava domes. *Bulletin of Volcanology*, **77**, 102, https://doi.org/10.1007/s00445-015-0986-z

Baxter, P.J., Bonadonna, C. *et al*. 1999. Cristobalite in volcanic ash of the Soufriere Hills Volcano, Montserrat, British West Indies. *Science (New York, NY)*, **283**, 1142–1145, https://doi.org/10.1126/science.283.5405.1142

Camejo-Harry, M., Pascal, K. *et al*. 2023. Monitoring volcano deformation at La Soufrière, St Vincent during the 2020–21 eruption with insights into its magma plumbing system architecture. *Geological Society, London, Special Publications*, **539**, https://doi.org/10.1144/SP539-2022-270

Casas, A.S., Wadsworth, F.B., Ayris, P.M., Delmelle, P., Vasseur, J., Cimarelli, C. and Dingwell, D.B. 2019. SO_2 scrubbing during percolation through rhyolitic volcanic domes. *Geochimica et Cosmochimica Acta*, **257**, 150–162, https://doi.org/10.1016/j.gca.2019.04.013

Cole, P.D., Robertson, R.E.A., Fedele, L. and Scarpati, C. 2019. Explosive activity of the last 1000 years at La Soufrière, St Vincent, Lesser Antilles. *Journal of Volcanology and Geothermal Research*, **371**, 86–100, https://doi.org/10.1016/j.jvolgeores.2019.01.002

Cole, P.D., Barclay, J. *et al*. 2023. Explosive sequence of La Soufrière, St Vincent, April 2021: insights into drivers and consequences via eruptive products. *Geological Society, London, Special Publications*, **539**, https://doi.org/10.1144/SP539-2022-292

Cronin, S.J., Stewart, C. *et al*. 2014. Volcanic ash leachate compositions and assessment of health and agricultural hazards from 2012 hydrothermal eruptions, Tongariro, New Zealand. *Journal of Volcanology and Geothermal Research*, **286**, 233–247, https://doi.org/10.1016/j.jvolgeores.2014.07.002

Damby, D.E. 2012. *From dome to disease: the respiratory toxicity of volcanic cristobalite*. PhD thesis, Department of Earth Sciences, Durham University, Durham, UK.

Damby, D.E., Horwell, C.J. *et al*. 2013. The respiratory health hazard of tephra from the 2010 Centennial eruption of Merapi with implications for occupational mining of deposits. *Journal of Volcanology and Geothermal Research*, **261**, 376–387, https://doi.org/10.1016/j.jvolgeores.2012.09.001

Damby, D.E., Llewellin, E.W., Horwell, C.J., Williamson, B.J., Najorka, J., Cressey, G. and Carpenter, M.A. 2014. The α-β phase transition in volcanic cristobalite. *Journal of Applied Crystallography*, **47**, 1205–1215, https://doi.org/10.1107/S160057671401070X

Damby, D.E., Murphy, F.A., Horwell, C.J., Raftis, J. and Donaldson, K. 2016. The in vitro respiratory toxicity of cristobalite-bearing volcanic ash. *Environmental Research*, **145**, 74–84, https://doi.org/10.1016/j.envres.2015.11.020

Damby, D.E., Horwell, C.J., Larsen, G., Thordarson, T., Tomatis, M., Fubini, B. and Donaldson, K. 2017. Assessment of the potential respiratory hazard of volcanic ash from future Icelandic eruptions: a study of archived basaltic to rhyolitic ash samples. *Environmental Health*, **16**, 98, https://doi.org/10.1186/s12940-017-0302-9

Damby, D.E., Horwell, C.J., Baxter, P.J., Kueppers, U., Schnurr, M., Dingwell, D.B. and Duewell, P. 2018. Volcanic ash activates the NLRP3 inflammasome in murine and human macrophages. *Frontiers in Immunology*, **8**, https://doi.org/10.3389/fimmu.2017.02000

Delmelle, P., Lambert, M., Dufrêne, Y., Gerin, P. and Óskarsson, N. 2007. Gas/aerosol–ash interaction in volcanic plumes: new insights from surface analyses of fine ash particles. *Earth and Planetary Science Letters*, **259**, 159–170, https://doi.org/10.1016/j.epsl.2007.04.052

Dollberg, D.D., Bolyard, M.L. and Smith, D.L. 1986. Evaluation of physical health effects due to volcanic hazards: crystalline silica in Mount St. Helens volcanic ash. *American Journal of Public Health*, **76**(3, Suppl.), 53–58, https://doi.org/10.2105/AJPH.76.Suppl.53

Eychenne, J., Gurioli, L. *et al*. 2022. Spatial distribution and physicochemical properties of respirable volcanic ash from the 16–17 August 2006 Tungurahua Eruption (Ecuador), and alveolar epithelium response in-vitro. *GeoHealth*, **6**, e2022GH000680, https://doi.org/10.1029/2022GH000680

Frost, G. 2013. The latency period of mesothelioma among a cohort of British asbestos workers (1978–2005). *British Journal of Cancer*, **109**, 1965–1973, https://doi.org/10.1038/bjc.2013.514

Govindaraju, K. 1994. 1994 compilation of working values and sample description for 383 geostandards. *Geostandards Newsletter*, **18**, 1–158, https://doi.org/10.1111/j.1751-908X.1994.tb00502.x

Heaney, P.J. 1994. Structure and chemistry of the low-pressure silica polymorphs. *Reviews in Mineralogy*, **29**, 1–40.

Hillman, S.E., Horwell, C.J., Densmore, A., Damby, D.E., Fubini, B., Ishimine, Y. and Tomatis, M. 2012. Sakurajima volcano: a physico-chemical study of the health consequences of long-term exposure to volcanic ash. *Bulletin of Volcanology*, **74**, 913–930, https://doi.org/10.1007/s00445-012-0575-3

Horwell, C.J. 2007. Grain size analysis of volcanic ash for the rapid assessment of respiratory health hazard. *Journal of Environmental Monitoring*, **9**, 1107–1115, https://doi.org/10.1039/b710583p

Horwell, C.J. and Baxter, P.J. 2006. The respiratory health hazards of volcanic ash: a review for volcanic risk mitigation. *Bulletin of Volcanology*, **69**, 1–24, https://doi.org/10.1007/s00445-006-0052-y

Horwell, C.J., Braña, L.P., Sparks, R.S.J., Murphy, M.D. and Hards, V.L. 2001. A geochemical investigation of fragmentation and physical fractionation in pyroclastic flows from the Soufriere Hills volcano, Montserrat. *Journal of Volcanology and Geothermal Research*, **109**, 247–262, https://doi.org/10.1016/S0377-0273(00)00319-X

Horwell, C.J., Michnowicz, S.A.K. and Le Blond, J.S. 2008. *Report on the Mineralogical and Geochemical Characterisation of Hawai'i Ash for the Assessment of Respiratory Health Hazard*. Report Issued to the USGS Hawaiian Volcano Observatory. International Volcanic Health Hazard Network.

Horwell, C.J., Le Blond, J.S., Michnowicz, S.A.K. and Cressey, G. 2010*a*. Cristobalite in a rhyolitic lava dome: evolution of ash hazard. *Bulletin of Volcanology*, **72**, 249–253, https://doi.org/10.1007/s00445-009-0327-1

Horwell, C.J., Stannett, G.W. *et al*. 2010*b*. A physicochemical assessment of the health hazard of Mt. Vesuvius volcanic ash. *Journal of Volcanology and Geothermal Research*, **191**, 222–232, https://doi.org/10.1016/j.jvolgeores.2010.01.014

Horwell, C.J., Williamson, B.J., Le Blond, J.S., Donaldson, K., Damby, D.E. and Bowen, L. 2012. The structure of volcanic cristobalite in relation to its toxicity; relevance for the variable crystalline silica hazard. *Particle and Fibre Toxicology*, **9**, 44, https://doi.org/10.1186/1743-8977-9-44

Horwell, C.J., Baxter, P.J. *et al*. 2013*a*. Physicochemical and toxicological profiling of ash from the 2010 and 2011 eruptions of Eyjafjallajökull and Grímsvötn volcanoes, Iceland using a rapid respiratory hazard assessment protocol. *Environmental Research*, **127**, 63–73, https://doi.org/10.1016/j.envres.2013.08.011

Horwell, C.J., Williamson, B.J., Llewellin, E.W., Damby, D.E. and Le Blond, J.S. 2013*b*. Nature and formation of cristobalite at the Soufrière Hills volcano, Montserrat: implications for the petrology and stability of silicic lava domes. *Bulletin of Volcanology*, **75**, 696, https://doi.org/10.1007/s00445-013-0696-3

Horwell, C.J., Hillman, S.E., Cole, P.D., Loughlin, S.C., Llewellin, E.W., Damby, D.E. and Christopher, T. 2014. Controls on variations in cristobalite abundance in ash generated by the Soufrière Hills volcano, Montserrat in the period 1997–2010. *Geological Society, London, Memoirs*, **39**, 399–406, https://doi.org/10.1144/M39.21

Huppert, H.E., Shepherd, J.B., Sigurdsson, H.R. and Sparks, R.S.J. 1982. On lava dome growth, with application to the 1979 lava extrusion of the Soufrière of St. Vincent. *Journal of Volcanology and Geothermal Research*, **14**, 199–222, https://doi.org/10.1016/0377-0273(82)90062-2

International Agency for Research on Cancer 1997. *Silica, Some Silicates, Coal Dust and Para-Aramid Fibrils*. International Agency for Research on Cancer, Lyon.

Ishida, T., Fujihara, N., Nishimura, T., Funabashi, H., Hirota, R., Ikeda, T. and Kuroda, A. 2019. Live-cell imaging of macrophage phagocytosis of asbestos fibers under fluorescence microscopy. *Genes and Environment*, **41**, 14, https://doi.org/10.1186/s41021-019-0129-4

IVHHN 2021. *Volcanic Ashfall Impacts on Water Supplies: Briefing Note*. International Volcanic Health Hazard Network.

IVHHN 2023. *Protocol for Analysis of Bulk Ash Samples for Health Hazard Assessment*. International Volcanic Health Hazard Network.

Joseph, E.P., Camejo-Harry, M. *et al*. 2022. Responding to eruptive transitions during the 2020–2021 eruption of La Soufrière volcano, St. Vincent. *Nature Communications*, **13**, 4129, https://doi.org/10.1038/s41467-022-31901-4

King, P.L., Ávila, J.N. *et al*. 2023. Sulfur isotopes in Kīlauea Volcano's 2018 summit ash: tracing sulfur-bearing reactions from the source to hydrothermal system and plume. Abstract presented at the IAVCEI 2023 Scientific Assembly, Rotorua, New Zealand.

Le Bas, M.J. and Streckeisen, A.L. 1991. The IUGS systematics of igneous rocks. *Journal of the Geological Society of London*, **148**, 825–833, https://doi.org/10.1144/gsjgs.148.5.0825

Le Blond, J.S., Cressey, G., Horwell, C.J. and Williamson, B.J. 2009. A rapid method for quantifying single mineral phases in heterogeneous natural dust using X-ray diffraction. *Powder Diffraction*, **24**, 17–23, https://doi.org/10.1154/1.3077941

Le Blond, J.S., Horwell, C.J. *et al*. 2010. Mineralogical analyses and in vitro screening tests for the rapid evaluation of the health hazard of volcanic ash at Rabaul volcano, Papua New Guinea. *Bulletin of Volcanology*, **72**, 1077–1092, https://doi.org/10.1007/s00445-010-0382-7

Lee, S.H. and Richards, R.J. 2004. Montserrat volcanic ash induces lymph node granuloma and delayed lung inflammation. *Toxicology*, **195**, 155–165, https://doi.org/10.1016/j.tox.2003.09.013

Leung, C.C., Yu, I.T.S. and Chen, W. 2012. Silicosis. *The Lancet*, **379**, 2008–2018, https://doi.org/10.1016/S0140-6736(12)60235-9

Leus, X., Kintanar, C. and Bowman, V. 1981. Asthmatic bronchitis associated with a volcanic eruption in St. Vincent, West Indies. *Disasters*, **5**, 67–69, https://doi.org/10.1111/j.1467-7717.1981.tb01130.x

Lipfert, F.W. and Wyzga, R.E. 2019. Longitudinal relationships between lung cancer mortality rates, smoking, and ambient air quality: a comprehensive review and analysis. *Critical Reviews in Toxicology*, **49**, 790–818, https://doi.org/10.1080/10408444.2019.1700210

Loomis, D., Grosse, Y. *et al*. 2013. The carcinogenicity of outdoor air pollution. *The Lancet Oncology*, **14**, 1262–1263, https://doi.org/10.1016/S1470-2045(13)70487-X

MacNee, W. and Donaldson, K. 2003. Mechanism of lung injury caused by PM_{10} and ultrafine particles with special reference to COPD. *European Respiratory Journal*, **21**(40 suppl):47s–51s, https://doi.org/10.1183/09031936.03.00403203

Miller, V.L., Joseph, E.P., Sapkota, J. and Szarzynski, J. 2022. Challenges and opportunities for risk management of volcanic hazards in small-island developing states. *Mountain Research and Development*, **42**, D22–D31, https://doi.org/10.1659/MRD-JOURNAL-D-22-00001.1

Morrison-Evans, B., Melekohva, E. and Blundy, J. 2023. Experimental insight into basaltic andesite lava dome oxidation textures at La Soufrière, St Vincent. *Geological Society, London, Special Publications*, **539**, https://doi.org/10.1144/SP539-2022-298

Nattrass, C., Horwell, C.J., Damby, D.E., Brown, D. and Stone, V. 2017. The effect of aluminium and sodium impurities on the cytotoxicity and pro-inflammatory potential of cristobalite. *Environmental Research*, **159C**, 164–175, https://doi.org/10.1016/j.envres.2017.07.054

Pan American Health Organization 2021. *La Soufriere Volcano, Situation Report #38, October 2021*. PAHO/WHO Office for Barbados and the Eastern Caribbean Countries, 5, https://www.paho.org/en/saint-vincent-and-grenadines

Phillips, J.C., Barclay, J., Cole, P.D., Johnson, M., Miller, V. and Robertson, R.E.A. 2023. Impacts and prospective hazard analysis of rainfall-triggered lahars on St Vincent 2021–22. *Geological Society, London, Special Publications*, **539**, in review.

Plail, M., Edmonds, M., Humphreys, M.C.S., Barclay, J. and Herd, R.A. 2014. Geochemical evidence for relict degassing pathways preserved in andesite. *Earth and Planetary Science Letters*, **386**, 21–33, https://doi.org/10.1016/j.epsl.2013.10.044

Reich, M., Zúñiga, A. *et al*. 2009. Formation of cristobalite nanofibers during explosive volcanic eruptions. *Geology*, **37**, 435–438, https://doi.org/10.1130/G25457A.1

Robertson, R. 2005. St Vincent. *In*: Lindsay, J.M., Robertson, R.E.A., Shepherd, J.B. and Ali, S. (eds) *Volcanic Hazard Atlas of the Lesser Antilles*. Seismic Research Unit, University of the West Indies, 240–261.

Schinwald, A., Murphy, F.A. *et al*. 2012. The threshold length for fiber-induced acute pleural inflammation: shedding light on the early events in asbestos-induced mesothelioma. *Toxicological Sciences*, **128**, 461–470, https://doi.org/10.1093/toxsci/kfs171

Schmid, O. and Stoeger, T. 2016. Surface area is the biologically most effective dose metric for acute nanoparticle toxicity in the lung. *Journal of Aerosol Science*, **99**, 133–143, https://doi.org/10.1016/j.jaerosci.2015.12.006

Stewart, C., Damby, D.E. *et al*. 2020. Assessment of leachable elements in volcanic ashfall: a review and evaluation of a standardized protocol for ash hazard characterization. *Journal of Volcanology and Geothermal Research*, **392**, 106756, https://doi.org/10.1016/j.jvolgeores.2019.106756

Stewart, C., Damby, D.E. *et al*. 2022. Volcanic air pollution and human health: recent advances and future directions. *Bulletin of Volcanology*, **84**, 11, https://doi.org/10.1007/s00445-021-01513-9

Stinton, A. 2023. Growth and evolution of the lava dome and coulée during the 2020–21 eruption of La Soufriere, St Vincent. *Geological Society, London, Special Publications*, **539**, https://doi.org/10.1144/SP539-2022-304

Surono, Jousset, P., Pallister, J. *et al*. 2012. The 2010 explosive eruption of Java's Merapi volcano – a '100-year'event. *Journal of Volcanology and Geothermal Research*, **241–242**, 121–135, https://doi.org/10.1016/j.jvolgeores.2012.06.018

Tomašek, I., Damby, D.E. *et al*. 2019. Assessment of the potential for in-plume sulphur dioxide gas-ash interactions to influence the respiratory toxicity of volcanic ash. *Environmental Research*, **179**, 108798, https://doi.org/10.1016/j.envres.2019.108798

Tomašek, I., Damby, D.E. *et al*. 2021. Development of a simulated lung fluid leaching method to assess the release of potentially toxic elements from volcanic ash. *Chemosphere*, **278**, 130303, https://doi.org/10.1016/j.chemosphere.2021.130303

Weber, G., Blundy, J. *et al*. 2023. Petrology of the 2020–21 effusive to explosive eruption of La Soufrière Volcano, St Vincent: insights into plumbing system architecture and magma assembly mechanism. *Geological Society, London, Special Publications*, **539**, https://doi.org/10.1144/SP539-2022-177

World Health Organization 1997. *Determination of Airborne Fibre Number Concentrations. A Recommended Method by Phase-Contrast Optical Microscopy*. World Health Organization, Geneva.

World Health Organization 2013. *Review of Evidence on Health Aspects of Air Pollution – REVIHAAP Project: Final Technical Report*. WHO European Centre for Environment and Health, Bonn, 302, https://www.euro.who.int/__data/assets/pdf_file/0004/193108/REVIHAAP-Final-technical-report-final-version.pdf